Defining the Fresnel zone for broadband radiation

Jeremy Pearce and Daniel Mittleman*
Department of Electrical and Computer Engineering, Rice University, MS-366, P.O. Box 1892, Houston, Texas 77251
(Received 10 April 2002; revised manuscript received 25 June 2002; published 15 November 2002)

The concept of the Fresnel zone is central to many areas of imaging. In tomographic imaging, the transverse spatial resolution can be limited by the size of the first Fresnel zone, usually defined only for monochromatic radiation. With the increasing prevalence of broadband tomographic imaging systems, a generalization of this concept is required. Here, a proposed generalization is described in the context of femtosecond optics, and experimentally verified using terahertz time-domain spectroscopy. Based on this definition, a simple zone plate design is demonstrated.

DOI: 10.1103/PhysRevE.66.056602 PACS number(s): 42.25.Fx, 42.30.Wb, 42.79.Ci

The concept of the Fresnel zone is a central one in wave propagation. The zone construction was first proposed by Fresnel in 1818, in an attempt to explain diffraction phenomena using Huygen's principle [1]. Although many authors have subsequently formulated equivalent descriptions, the ongoing importance of the notion of a Fresnel zone is best illustrated by the following scenario. Consider a spherical wave incident on a reflecting circular target. Each element of the target's surface generates a reflected spherical wave; the net disturbance at the location of a detector consists of the coherent sum of all these reflected waves. As a specific example, assume that the locations of the emitter and detector are the same [Fig. 1(a)]. If the two-way path difference $\Delta L = 2(\rho - z)$ is less than $\lambda/2$, then all the reflected waves constructively interfere. On the other hand, waves originating from the annular region for which $\lambda/2 < \Delta L < \lambda$ contribute to the detected signal with opposite sign, resulting in partial destructive interference. Successively larger annular regions contribute with alternating signs, resulting in a well-defined progression of reflecting zones [1]. The first Fresnel zone is traditionally defined as the largest reflecting disk for which all reflected waves reach the detector with phase shifts $\Delta\phi \leqslant \pi$. From the geometry of Fig. 1, this implies that the radius of this first zone is given by

$$r_F = \frac{\lambda}{4}\sqrt{1+(8z/\lambda)} \approx \sqrt{z\lambda/2}. \tag{1}$$

where the approximate form assumes that $z \gg \lambda$.

This analysis has one of its most important implications in the context of imaging. In a tomographic imaging system, in which an incident (e.g., spherical) wave is reflected from a target and then detected at numerous locations, the target must be at least as large as the first Fresnel zone of the incident wave in order to be resolved. This concept has been discussed extensively in the context of acoustic imaging, particularly for the case of geophysical seismic imaging [2–6], and also in other situations such as ultrasonic imaging [7] and helioseismology [8]. These considerations also apply to other types of wave propagation phenomena, including such diverse areas as millimeter-wave and submillimeter-wave optical imaging [9–11], microwave communications [12], holography [13], and atom optics [14].

In many of these examples, the relevant propagating fields are broadband in nature. This immediately leads to a difficulty, since the traditional description of the Fresnel zone [e.g., Eq. (1)] applies to monochromatic fields, and is not readily generalized to the case of broadband radiation. Several generalizations of the definition of the Fresnel zone have been proposed by researchers in the seismic imaging community [15,16]. The optical analog, in which plane or spherical waves are incident on either a circular reflector or a circular hole in a reflecting screen, has been studied in great detail by numerous authors, but only for the case of monochromatic radiation [17]. To our knowledge, the extension to the broadband case has not been discussed at all for electromagnetic waves. Even in the case of acoustic waves, no controlled experimental studies have been reported. Here, we provide a simple generalization for the case of broadband optical pulses, which is analogous to the proposal for seismic waves advanced by Brühl, Vermeer, and Kiehn [16]. We employ terahertz time-domain spectroscopy to obtain experimental results for comparisons with this theory. Although formulated in the context of femtosecond optics, these results are quite general, and are applicable to any tomographic imaging problem that relies on broadband fields.

For an arbitrary spherical wave $E(t)$ emitted towards a circular reflector (see Fig. 1), the reflected field at the position of the emitter can be determined using the Kirchhoff diffraction integral. This field consists of two replicas of the input wavelet, one from the center of the reflector and another, scaled and inverted, from its edge:

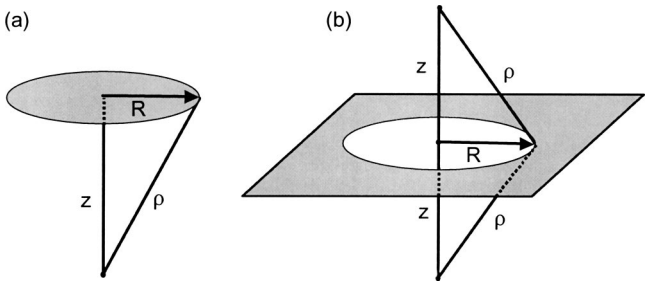

FIG. 1. Schematics of (a) the reflection and (b) the transmission geometries relevant to the discussions in the text.

*FAX: (713) 348-5686. Email address: daniel@rice.edu

$$E_{\mathrm{det}}(t) \propto E(t-T_0) - \frac{z^2}{\rho^2} E(t-T), \tag{2}$$

where T_0 is the two-way travel time to the center of the reflector and T is the two-way travel time to the edge [18]. If the emitted field is a Gaussian pulse, so that $E(t) \propto \exp(-t^2/t_w^2)\exp(i\omega t)$, then the total energy reaching the receiver, $S = \int |E_{\mathrm{det}}(t)|^2 dt$, is given by

$$S \propto 1 + \frac{z^4}{\rho^4} - \frac{2z^2}{\rho^2} e^{-\tau^2/2t_w^2} \cos \omega\tau. \tag{3}$$

Here, $\tau = T - T_0 = 2(\rho - z)/c$ is the temporal separation between the two reflected wavelets. For small reflector radii, this function increases in proportion to the reflector area, as expected. For larger radii, the total energy reaches a maximum and then oscillates as the reflector size increases; the oscillations decrease in amplitude and then disappear as the two pulses in Eq. (2) become temporally separated. These alternating maxima and minima correspond to constructive and destructive interference, reflecting the addition of consecutive Fresnel zones to the reflector. It is fairly straightforward to demonstrate that the same result is obtained if the pulses are chirped, or indeed even if incoherent radiation is employed. The energy reaching the detector does not depend on the temporal phase of the input wavelet, but only on the spectral bandwidth.

As noted by several authors, it is clear that, for sufficiently short pulses (relative to $1/\omega$), the oscillatory structure vanishes, and only a single maximum remains [3,16]. In this situation, only the first Fresnel zone can be defined, and all higher zones become meaningless. In essence, the path length difference ΔL is less than the coherence length of the light for only the first Fresnel zone, so only the radiation diffracted from the first zone boundary gives rise to constructive interference. The size of the first Fresnel zone may therefore be defined as the radius of the reflector for which the maximum energy reaches the detector. This quantity is well defined even for single- or half-cycle pulses. Further, it is a more reasonable choice than others proposed [4,15], since it reduces to the correct limit [Eq. (1)] for narrowband radiation. Indeed, although no closed-form solution can be obtained from Eq. (3) for the size of the first Fresnel zone, numerical analysis demonstrates that it depends only weakly on the spectral bandwidth, and furthermore that it varies approximately as the square root of the mean wavelength, as expected.

Although the problem of optical diffraction through a circular aperture has been considered by many authors, starting with Rayleigh in 1897 [17], we are not aware of any explicit experimental observation that illustrates the two distinct temporal wavelets described by Eq. (2). This is, in part, a consequence of the fact that the vast majority of the research in diffraction theory has considered only monochromatic fields. In light of the above discussion, which clarifies the distinctions between the monochromatic and broadband situations, an experimental demonstration of this phenomenon provides a useful illustration. In order to directly verify Eq. (2), we employ terahertz time-domain spectroscopy, which permits direct measurement of the diffracted electric field with high temporal resolution. This system produces single-cycle electromagnetic pulses, with spectral content spanning the range of wavelengths from 300 μm to 3 mm. We use the diffraction geometry shown in Fig. 1(b); using Babinet's principle, it is clear that the measured fields are identical to those that would be measured in the reflection geometry [Fig. 1(a)]. The terahertz spectrometer is similar to the one described previously [10,19]. The emitter and receiver both employ aplanatic hyperhemispherical substrate lenses, which produce a beam that approximates a spherical wave, at least within a $\sim 15°$ cone (half-angle) around the optic axis [19]. The emitter and receiver are positioned 456 mm apart, and a thin metal diaphragm positioned half way between is used as a variable aperture.

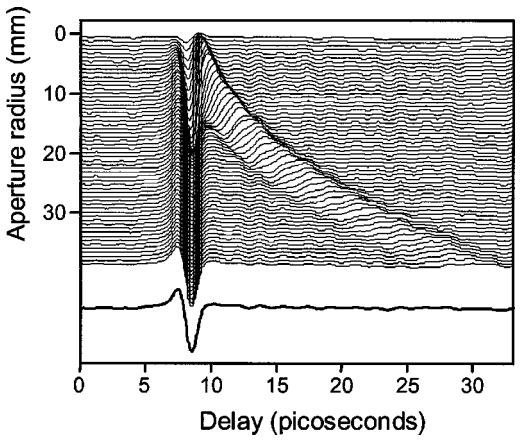

FIG. 2. A series of terahertz wave forms transmitted through a planar circular aperture. These are plotted in arbitrary units; the vertical axis indexes the radius of the aperture for each wave form. The offset wave form at the bottom of the figure is a reference, measured with no aperture in the beam path.

Figure 2 shows the measured terahertz wave forms as a function of the aperture radius. The edge-diffracted pulse, moving to larger delay with increasing aperture size, is clearly visible. Figure 3 shows the total received energy as a function of aperture radius. The solid line represents a computation of $\int |E_{\mathrm{det}}(t)|^2 dt$ using an experimental reference pulse (measured with no aperture) as the wavelet in Eq. (2). The radius of the Fresnel zone, as indicated by the location of the peak signal, agrees well with the predicted value. The vertical arrow indicates the location of the maximum predicted by Eq. (1) with λ replaced by $\langle\lambda\rangle = 0.95$ mm, the mean wavelength. Simply using the mean pulse wavelength overestimates the size of the Fresnel zone by $\sim 8\%$ in this case. For large aperture radii, the integrated signal is somewhat smaller than that predicted by Eq. (2), probably because of the loss of higher frequency components of the wavelet due to slight misalignment of the detector antenna or of the aperture.

We can use this understanding of the nature of the Fresnel zone to design new optical components suitable for broadband radiation. For example, since a propagating wave front consisting of a single-cycle pulse contains only one Fresnel zone, a zone plate is easily fabricated since one need only consider the first zone. The advantages of zone plates over

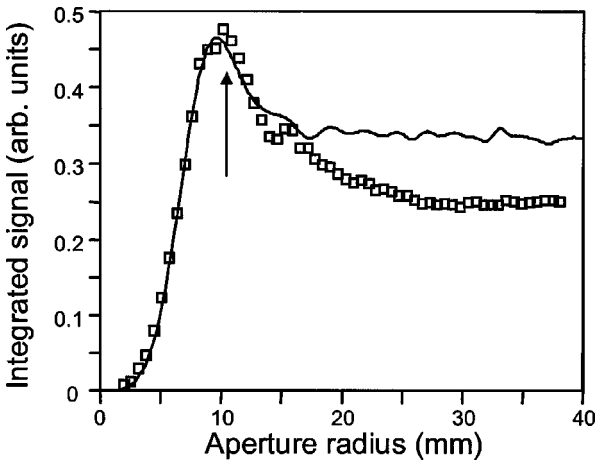

FIG. 3. The total energy reaching the detector as a function of aperture radius. The open squares represent the data from Fig. 2. The solid curve shows the result computed from the reference wave form (bottom of Fig. 2) using Eq. (2). The arrow shows the location of the first Fresnel zone predicted by Eq. (1) using the spectrum-weighted mean wavelength.

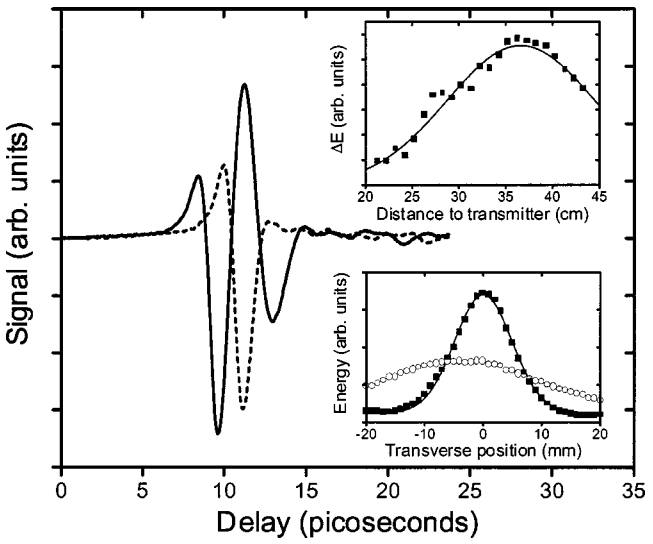

FIG. 4. The solid curve shows the wave form measured at the focus of a single-zone Fresnel lens as described in the text. The smaller dashed curve shows the wave form measured at the same location, when the lens is replaced by a polyethylene flat of equivalent thickness. The lower inset shows the energy in the beam as a function of transverse position, both with (solid squares) and without (open circles) the lens. The solid curve through the squares is a Gaussian with a width determined by convolving two Gaussian functions representing the transmitter and receiver apertures. The correspondence between this curve and the data indicates that the focus is diffraction limited, with a beam waist of 7.8 mm. The upper inset shows the results of a longitudinal scan, along the beam propagation direction. Plotted is the difference in the total energy between the beam propagating through the lens and through an optical flat. The peak demonstrates the longitudinal focus. The width of this focus is extracted using a Gaussian fit (solid curve), resulting in a Rayleigh range of 9.3 mm.

conventional lenses are numerous and well documented, and the fabrication of such optical components for far infrared and millimeter-wave applications is an active area of research [11,20]. We create a Fresnel lens by milling a circular depression at the center of a thin polyethylene plate. The radius of this depression, the Fresnel zone radius, is chosen to be 9.525 mm (3/8 in.) for convenience of machining. This choice, along with the value of $\langle\lambda\rangle$, fixes the transmitter-to-lens distance according to Eq. (1), $z=191$ mm. The depth of the depression, 0.904 mm, is chosen to provide a π phase shift for the wave front traveling through this milled region.

The focusing action of this simple lens is illustrated in Fig. 4. This shows two wave forms, one measured with a single-zone Fresnel lens in the beam and the other with a polyethylene flat in the beam. In both cases, the transmitter is located, as in Fig. 1(b), 191 mm from the lens. In this configuration, the lens images the transmitter onto the receiver, which is situated at the primary focal point. The energy in the focused terahertz field (solid curve) is more than twice that of the unfocused expanding spherical wave (dashed curve).

We also characterize the beam focus by translating the receiver through the focus, along a line perpendicular to the propagation direction. In a one-to-one imaging configuration of this sort, the focal spot size is expected to be equal to the effective size of the transmitter. The measured focal spot profile should therefore be approximately Gaussian, with a width given by the convolution of the transmitter and receiver apertures. Figure 4 (lower inset) shows the total energy in the measured wavelets, as a function of position across the focal spot. The solid line is a Gaussian, with width determined by the appropriate convolution. The excellent agreement between the measured and predicted focal spot sizes demonstrates that the focus is diffraction limited. The open circles show the equivalent result when the lens has been replaced with the featureless polyethylene flat, indicating the relatively weak dependence on position for the unfocused beam.

Finally, we scan the receiver along the optic axis through the focal spot, both with the lens and with the flat, to observe the longitudinal focusing. The upper inset in Fig. 4 shows the difference in total energy between the two cases as a function of the transmitter-to-receiver distance. These data extend to a distance of 433 mm limited by the length of our optical delay line. The solid curve is a Gaussian fit to these data, showing a clear maximum at the location of the focus. The width of this Gaussian is a measure of the Rayleigh range of the focusing beam, which can also be computed independently from the measured beam waist. From the transverse scan (lower inset), we extract a waist of $w=7.8$ mm. Then, the Rayleigh range can be computed according to $\pi w^2/2\langle\lambda\rangle$. This gives a value of 9.5 mm, quite similar to the value of 9.3 mm extracted from the longitudinal scan (upper inset).

In conclusion, we describe an extension of the Fresnel zone concept for broadband radiation. This has important implications for tomographic imaging applications, where the longitudinal (depth) resolution is determined by the coherence length of the radiated field. A short coherence length, valuable for improved depth resolution, necessarily leads to some difficulty in defining the transverse resolution. In addi-

tion to addressing this issue, we also propose and demonstrate a design for a Fresnel lens optimized for broadband fields. This exceedingly simple design could prove valuable in infrared and microwave imaging applications. Based on the above discussion, adding additional zones to the lens should not provide substantial improvement in the spatiotemporal focusing of these broadband pulses, unless a more complicated lens design is employed [11].

[1] M. Born and E. Wolf, *Principles of Optics* (Cambridge University Press, Cambridge, UK, 1999).
[2] R. E. Sheriff, Geophysics **45**, 968 (1980).
[3] O. Gudmundsson, Geophys. J. Int. **124**, 304 (1996).
[4] J. Schleicher *et al.*, Geophysics **62**, 183 (1997).
[5] P. D. Thore and C. Juliard, Geophysics **64**, 593 (1999).
[6] J. Sun, Geophys. Prospect. **47**, 1045 (1999).
[7] D. W. Schindel, A. G. Bashford, and D. A. Hutchins, IEEE Trans. Ultrason. Ferroelectr. Freq. Control **46**, 242 (1999).
[8] A. C. Birch *et al.*, Astrophys. J. Lett. **561**, 229 (2001).
[9] A. W. Rihaczek, *Principles of High-Resolution Radar* (McGraw-Hill, New York, 1969).
[10] T. D. Dorney *et al.*, Opt. Lett. **26**, 1513 (2001).
[11] S. Wang, T. Yuan, E. D. Walsby, R. J. Blaikie, S. M. Durbin, D. R. S. Cumming, J. Xu, and X.-C. Zhang, Opt. Lett. **27**, 1183 (2002).
[12] L. C. Andrews *et al.*, J. Opt. Soc. Am. A **16**, 1417 (1999).
[13] L. Bergmann and C. Schaefer, *Optics of Waves and Particles* (Walter de Gruyter, Berlin, 1999).
[14] R. B. Doak *et al.*, Phys. Rev. Lett. **83**, 4229 (1999).
[15] R. W. Knapp, Geophysics **56**, 354 (1991).
[16] M. Brühl, G. J. O. Vermeer, and M. Kiehn, Geophysics **61**, 600 (1996).
[17] See for example J. W. Miles, J. Appl. Phys. **20**, 760 (1949), and references therein.
[18] B. R. Zavalishin, Geophys. Prospect. **48**, 631 (2000).
[19] J. V. Rudd and D. M. Mittleman, J. Opt. Soc. Am. B **19**, 319 (2002).
[20] J. C. Wiltse, Proc. SPIE **4111**, 201 (2000).